Mode Count and Modal Density of Isotropic Circular Cylindrical Shells Using a Modified Wavenumber Space Integration Method

Mohammad H. Farshidianfar[1]
Master of Applied Science Candidate
Department of Mechanical and Mechatronics Engineering,
University of Waterloo,
Waterloo, ON N2L 3G1, Canada
e-mail: mhfarshi@uwaterloo.ca

Anooshiravan Farshidianfar
Professor
Department of Mechanical Engineering,
Ferdowsi University of Mashhad,
Mashhad, Iran
e-mail: farshid@um.ac.ir

Mahdi Mazloom Moghadam
Master of Applied Science Candidate
Department of Mechanical Engineering,
Ferdowsi University of Mashhad,
Mashhad, Iran
e-mail: mah.mazloom.mo@gmail.com

A new method based on the wavenumber space integration algorithm is proposed in order to obtain mode count and modal density of circular cylindrical shells. Instead of the simplified equation of motion, the exact equation is applied in mode count calculations. Modal plots are changed significantly in the k-space when using the exact equation. Mode repetition in cylindrical shells is represented by additional mode count curves in the k-space. On the other hand, a novel technique is presented in order to implement boundary condition effects in mode count and modal density calculations. Integrating these two significant corrections, a modified wavenumber space integration (MWSI) method is developed. Mode count and modal densities of three shells with different geometrical and acoustical properties are obtained using the MWSI method and conventional WSI. Results are verified using the exact mode count calculations. Moreover, effects of geometrical properties are studied on mode count plots in the k-space. Modal densities are obtained for cylindrical shells of different lengths, radii, and thicknesses. Finally, modal densities of cylindrical shells are compared to flat plates of the same size and boundary condition. Interesting results are obtained which will contribute in calculation of acoustic radiation efficiency and sound transmission in cylindrical shells.
[DOI: 10.1115/1.4027212]

Keywords: mode count, modal density, modified wavenumber space integration, circular cylindrical shell, resonance frequency

1 Introduction

The dynamics of simple structural elements, such as plates and shells, has attracted a great deal of attention in several branches of engineering. These include acoustical and vibration engineering. Analysis of noise transmission and structure-borne sound in the aerospace industry, electric motor casings, and pipes are only a few of the main applications in this field. Since these structures are normally opposed to high frequency excitation, the statistical energy analysis (SEA) is used to anticipate their response. To predict the result in SEA, three main parameters: (1) modal density, (2) coupling loss factor, and (3) dissipation loss factor have to be defined. The modal density is expressed as the average number of modes in a unit frequency. The problem of determining the modal density of an acoustical cavity is obtained through analysis of its eigenvalue distributions. The distribution of these eigenvalues is usually expressed as mode count of an acoustical cavity. Mode count is the total number of modes below a given frequency. The differentiation of the mode count with respect to frequency then yields the modal density.

Previous researchers have conducted initial investigations on the modal density and mode count of beams, plates, and shells [1–6]. Courant and Hilbert [7] studied the asymptotic distribution of eigenvalues for various dynamic systems by developing the wavenumber space integration (WSI) method. Bolotin [8] corrected Courant and Hilbert's [7] work by introducing the effect of edge conditions on shell's mode shapes. He later presented a more detailed study into the asymptotic behavior of the eigenvalues for a generalized plate [9] and a generalized elastic shell [10]. Although Bolotin did mention the effects of boundary conditions on mode shapes and natural frequencies, but he did not mention boundary condition effects on the modal density and mode count plots. Heckl [11] also developed similar expressions to Bolotin for natural frequency of cylindrical shells. He also presented a closed form solution for mode count and modal density of shells; however, in his report, the modal density is only a function of size of the system.

Szechenyi [12] provided the mode count and modal density of cylindrical shells by means of a graphical integration method similar to the WSI. He used the modal density plots to find radiation efficiency and sound transmission of cylindrical shells. Maymon [13] generalized Szechenyi's [12] work by introducing eccentric stiffeners and axial load to the model. He concluded that by increasing the eccentricity of the stiffeners in a more compact area the modal density of a cylindrical shell could be reduced to one fourth. Ramachandran and Narayanan [14] also studied the effects of stiffeners on the modal density of cylindrical shells using a more deterministic approach rather than the graphical WSI method. Several other researchers [15–19] have applied the WSI method in order to obtain modal properties and sound transmission of cylindrical shells. Xie et al. [20] developed a WSI method for mode count and modal density calculations of bars and plates. In their research, they proposed a new method in order to introduce the effects of boundary conditions on the final mode count calculations. They were also able to produce closed form solutions for mode count and modal density of bars and plates.

The WSI method is widely applied for modal analysis of cylindrical shells, however; one of the main setbacks of this technique is its independency of boundary conditions. Many researchers

[1]Corresponding author.

Contributed by the Design Engineering Division of ASME for publication in the Journal of Vibration and Acoustics. Manuscript received September 9, 2013; final manuscript received March 13, 2014; published online April 18, 2014. Assoc. Editor: Marco Amabili.

[12,14,17–19] have utilized the WSI method to obtain radiation efficiencies and acoustical properties of cylindrical shells. Radiation efficiency is known to be a function of boundary conditions, but the effect of boundary conditions on the mode count and modal density of cylindrical shells has received no significant attention. There is no report available in literature for cylindrical shells expressing the dependency of modal density on shells' boundary conditions. However, boundary conditions affect mode shapes and modal distribution of cylindrical shells [21]. Moreover, since dynamic equations of a cylindrical shell are complicated, simplified versions of the equation of motion are used in the conventional WSI method. Such simplifications underestimate modal distribution of a shell, thus providing several sources of error in mode count and modal density calculations. Therefore, there are a couple shortcomings when applying the WSI method especially to complicated acoustical cavities such as cylindrical shells.

The aim of the present paper is to develop a modified wavenumber space integration (MWSI) method for cylindrical shells using the exact equation of motion. The developed method will consider the effects of boundary conditions on the shell's mode count and modal density. First, equations of motion are developed for a plate and cylindrical shell. The conventional WSI method is described for cylindrical shells, pointing out the current shortcomings of the method. In order to correct the conventional WSI, an MWSI method is proposed in two steps. In the first step, the simplified equation of motion is replaced with the exact equation. Significant changes to the modal curves and their final effects on the mode count and modal density are explained in full detail. Next, a novel technique is developed in the k-space (wavenumber space) in order to introduce the effects of boundary conditions in the MWSI method. Results of the MWSI and conventional WSI methods are compared with exact calculation of the mode count. Mode counts of three types of cylindrical shells with different geometrical properties are studied in order to investigate the generality of the MWSI technique. The effects of boundary conditions and applying the exact equation are identified on the final mode count. After the method is verified, modal density plots are obtained for the cylindrical shells using the MWSI and WSI techniques. The effects of shell geometrical properties, such as length, radius and thickness, are also studied in mode count distributions of cylindrical shells. Modal density plots are compared for shells of different geometries. Finally, modal densities of cylindrical shells are compared to flat plates. The results will contribute in modal analysis and calculation of sound transmission through cylindrical shells.

2 Resonance Frequencies

2.1 Resonance Frequencies of Flat Plates. Consider a flat plate with dimensions $a \times b$. The coordinates are vertically in y-direction and horizontally in the x-direction. The equation of motion for the bending waves of a flat plate with thickness h is given as follows:

$$D\left[\frac{\partial^4 W}{\partial x^4} + 2\frac{\partial^4 W}{\partial x^2 \partial y^2} + \frac{\partial^4 W}{\partial y^4}\right] + \rho h \frac{\partial^2 W}{\partial t^2} = 0 \tag{1}$$

in which $D = Eh^3/12(1-\upsilon^2)$ is termed as the bending stiffness of a flat plate. In Eq. (1), E, υ, ρ, and w are the plate's Young's modulus, Poisson's ratio, density, and out of plane displacement, respectively. Consider a harmonic plane wave in the following form:

$$W(x,y,t) = Ae^{-ik_x x}e^{-ik_y y}e^{i\omega t} \tag{2}$$

where k_x and k_y are structural wavenumbers in the x and y directions, respectively. Substituting Eq. (2) into Eq. (1) yields

$$D[k_x + k_y]^2 - M\omega^2 = 0 \tag{3}$$

in which M is the mass per unit area of the plate. It is noticed that the characteristic equation of a flat plate (Eq. (3)) is a simple second degree polynomial equation in terms of frequency. Thus, for each mode pair of k_x and k_y, there exists a single resonance frequency.

2.2 Resonance Frequencies of Cylindrical Shells. Consider a cylindrical shell with thickness h, mean radius R, and axial length l as shown in Fig. 1. The mechanical properties c, υ, and ρ are expressed similar to the plate (Sec. 2.1). Since the displacements for a shell are not as simple as a plate, the equation of motion according to the Flugge theory [21] is represented in a matrix form as follows:

$$\begin{bmatrix} L_{11} & L_{12} & L_{13} \\ L_{21} & L_{22} & L_{23} \\ L_{31} & L_{32} & L_{33} \end{bmatrix} \begin{Bmatrix} u \\ v \\ w \end{Bmatrix} = 0 \tag{4}$$

where u, v, and w are orthogonal directions in the axial, circumferential, and radial directions, respectively, as shown in Fig. 1. L_{ij} $(i, j = 1, 2, 3)$ are differential operators with respect to x and θ. Assume the following distortion functions for the cross section of the shell:

$$\begin{cases} u = A\cos(k_a x)\cos(n\theta)\cos(\omega t) \\ v = B\sin(k_a x)\sin(n\theta)\cos(\omega t) \\ w = C\sin(k_a x)\cos(n\theta)\cos(\omega t) \end{cases} \tag{5}$$

in which k_a and n are the axial wavenumber and the circumferential wave parameter, respectively. Moreover, A, B, and C are the modal (wave) amplitudes in the x, θ, and z directions, respectively, with a circular driving frequency of ω. Substituting Eq. (5) into Eq. (4) and equating the determinant of the coefficient matrix to zero, the following is yield as the characteristic equation of a cylindrical shell:

$$\Omega^6 - (p_4)\Omega^4 + (p_2)\Omega^2 - (p_0) = 0 \tag{6}$$

in which

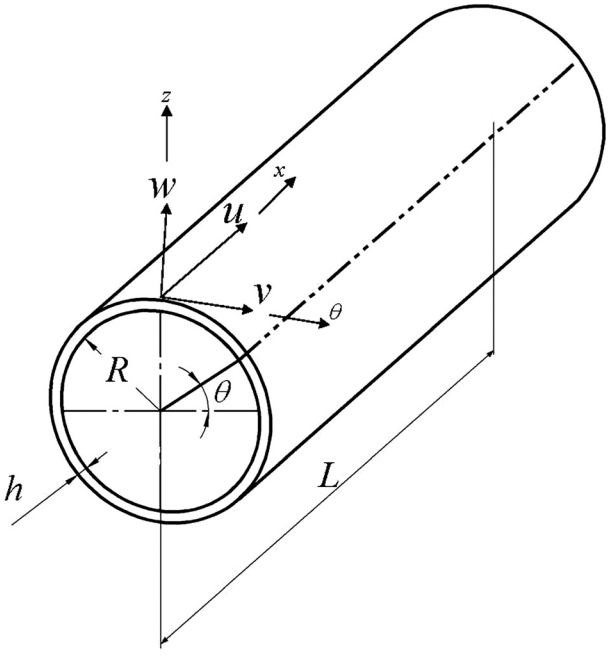

Fig. 1 Circular cylindrical shell: coordinate system and dimensions

$$\Omega^2 = \frac{\rho(1-\upsilon^2)R^2\omega^2}{E}, \quad \beta = \frac{h^2}{12R^2} \tag{7}$$

are the nondimensional frequency and nondimensional thickness parameter, respectively. In the above, p_i ($i = 0, 2, 4$) are functions of k_a and n which are given in the Appendix. Thus, a different characteristic equation (Eq. (6)) is obtained for every boundary condition, since k_a and n are functions of the shell boundaries. It is interesting that the characteristic equation of a cylindrical shell (Eq. (6)) is a 6th degree polynomial equation in terms of the driving frequency. Hence, for each combination of k_a and n which represent one mode, there exists three positive roots to the bicubic Eq. (6). As a result, every mode shape is repeated at three distinct frequencies, each having a primarily radial (or flexural), longitudinal (or axial), or circumferential (or torsional) motion [21]. As explained earlier, the only unknowns in Eq. (6) are k_a and n, which are hidden in the p_i ($i = 0, 2, 4$) terms. One could rearrange Eq. (6) in the following form:

$$k_a^8 + q_6 k_a^6 + q_4 k_a^4 + q_2 k_a^2 + q_0 = 0 \tag{8}$$

where q_i ($i = 0, 2, 4, 6$) are functions of ω and n this time. Comparing Eq. (3) with Eq. (8), it is interesting that the plate characteristic equation (Eq. (3)) is a 2nd degree equation in terms of the wavenumbers whereas, Eq. (8) is an 8th degree polynomial. This is why the modal distribution of a cylindrical shell is much more complicated and hard to analyze, compared to a flat plate.

2.1.1 Simplified Characteristic Equation for a Cylindrical Shell. Since the 6th degree polynomial of Eq. (6) is complicated to analyze, there have been several simplifications applied to find easier solutions to the equation [22]. One of the most broadly used simplified equations is proposed by Soedel [23]. According to Soedel's formulae, the resonance frequencies of a cylindrical shell are given by

$$\omega_{mn} = \left[D(k_a^2 + k_c^2)^2 + \frac{k_x^4}{(k_x^2 + k_c^2)^2} \right]^{1/2} .2\pi f_r \tag{9}$$

in which

$$f_r = \left(\frac{1}{2\pi R}\right)\sqrt{\frac{E}{\rho_m}} \text{(ring frequency)} \tag{10}$$

is defined as the ring frequency. k_a and k_c are the axial and circumferential wavenumbers, respectively. The circumferential wavenumber is another form of representation for the circumferential waveparameter, defined by $k_c = (n/R)$. The ring frequency, which is also termed as the breathing mode, is one of the most important frequencies in cylindrical shells. At the ring frequency, the shell undergoes uniform expansions and contractions with $n = 0$. At this frequency, radial hooplike resonance occurs [17].

The Soedel simplified equation does not take into account two of the three resonance frequencies, since it is a 2nd degree polynomial whereas the exact characteristic equation is a 6th degree. In a more detailed study, Farshidianfar et al. [21] compared results of the exact and simplified equations with experimental data. It was observed that the simplified version of the equation yields high errors, whereas the exact equation predicted frequencies with great accuracy. However, because of its simple nature, Eq. (9) has been widely utilized to obtain mode counts and modal densities of cylindrical shell in the WSI method. From this section, forward Eq. (6) will be termed as the "exact equation" and Eq. (9) as the "simplified equation."

2.3 Wavenumber Identification. In the above sections, three characteristic equations (Eqs. (3), (6), and (9)) were obtained for a flat plate (Eq. (3)) and cylindrical shell (Eqs. (6) and (9)). In all these equations, there exists wavenumber terms identified by k_x, k_y, k_a, and k_c. In order to solve the characteristic equation in terms of frequency, one has to treat these wavenumbers as known variables. The three wavenumbers, which are in longitudinal direction k_x, k_y, and k_a, are of the same type for both plate and shell vibration. Therefore, it is assumed that they will be defined by a similar function. The flexural mode shapes of flat plates and cylindrical shells in the longitudinal direction are assumed to be of the same form as a transversely vibrating beam, with the same boundary conditions. Modal wavenumbers in the longitudinal direction (k_x, k_y, and k_a) for different boundary conditions are presented in Table 1. These modal wavenumbers are according to the beam functions with identical boundary conditions as the plate or the shell.

The validity and accuracy of using beam functions as replacements of modal wavenumbers in the longitudinal direction were studied and proved in a recent study by Farshidianfar et al. [24,25]. It is noteworthy that in Table 1, there exists an extra $(\pi/2)$ term for the clamped conditions. The inclusion of this term will convert all sinusoidal displacements in Eq. (5) into cosine displacements, which is expected in clamped boundary conditions. Therefore, k_a is defined according to beam functions for each boundary condition that will result in a different distortion function (Eq. (5)) and different characteristic equation (Eq. (6)) for every boundary condition.

The circumferential wavenumber of a cylindrical shell, which is defined by $k_c = (n/R)$ is not a function of the shell boundaries. In general, n which is the only unknown in k_c obtains integer values ($n = 0, 1, 2, \ldots$), independent of boundary conditions.

3 Mode Count and Modal Density

The total number of modes existing below a specific frequency is called the mode count. Since it is normally plotted as a function of frequency or wavenumber, mode count plots usually form a staircase diagram. Although the staircase function is the actual distribution of the modes, to be more useful, researchers usually use an average form of the staircase. The average mode count is calculated as follows [20]:

$$N(k) = \eta - \frac{1}{2} \tag{11}$$

in which η represents the normal mode count. The differentiation of $N(k)$ with respect to frequency, results in the modal density, $n(k)$. In other words, the modal density is given by

$$n(k) = \frac{dN(k)}{d\omega} \tag{12}$$

Generally, modal density is defined as the total number of modes in a frequency band with units (modes/Hz).

For the case of 3D acoustical cavities, such as flat plates and cylindrical shells, the mode count is calculated by plotting the frequency equation in the k-space. In this method, the frequency at which the mode count is to be obtained is assumed to be known and inserted into the characteristic equation and thus only the wavenumbers (axial and circumferential) will be the variables. Therefore, the characteristic equation for the mentioned frequency

Table 1 Shell axial wavenumbers according to beam functions

Plate/shell boundaries	Wavenumber
Simply supported–simply supported (SS–SS)	$k_x = k_y = k_a = \frac{m\pi}{l}$ $(m = 1, 2, 3, \ldots)$
Clamped–clamped (C–C)	$k_x = k_y = k_a = \frac{(2m+1)\pi}{2l}$ $(m = 1, 2, 3, \ldots)$

will be plotted as functions of the two varying wavenumbers. Thus, the k-space for flat plate is plotted in the k_x–k_y and for a cylindrical shell in the k_a–k_c space. The area below this k-space plot would be calculated and divided by the area occupied by each mode to obtain the mode count. This method is called the WSI method. The WSI will be explained graphically for flat plates and cylindrical shells in detail in Sec. 5.1.

4 Mode Count and Modal Density of Flat Plates

The k-space plot of a SS–SS flat plate is presented in Fig. 2. The mode count of a plate below a specific frequency is given by the number of modes lying underneath the wavenumber curve, which is given by

$$N(k) = \frac{\int_s dk_x dk_y}{\Delta k_x \Delta k_y} \tag{13}$$

where S is the area of integration, Δk_x and Δk_y are the change in axial wavenumbers from one mode to the next. According to the values presented in Table 1, each mode occupies an area of $(\pi/a) \times (\pi/b)$. In Fig. 2, each mode has been indicated by a square mark. According to Eq. (13), all modes below the curve should be taken into account for the mode count below a certain frequency. However, by separating a square of $(\pi/a) \times (\pi/b)$ around each mode, it is shown that the integration of Eq. (13) should be calculated under a transformed coordinate axes $k_x' - k_y'$ instead of the original k_x–k_y. According to Fig. 2, identifying each mode with a box of size $(\pi/a) \times (\pi/b)$, a half strip along the k_x and k_y axis should not be taken into account for mode count calculations. Xie et al. [20] applied the above procedure by subtracting two half strips from the final integration of Eq. (13). They obtained the following closed form solutions for mode counts of a flat plate [20]:

$$N(k) = \frac{k^2 S}{4\pi} - \frac{1}{4\pi} kP + \frac{1}{4} \quad \text{All edges simply supported} \tag{14}$$

$$N(k) = \frac{k^2 S}{4\pi} - \frac{1}{2\pi} kP + 1 \quad \text{All edges clamped} \tag{15}$$

in which $P = 2(a+b)$ and $S = ab$ are the plates' perimeter and area, respectively. Such closed form solutions were yield since the mode curve of a flat plate is in the form of a quarter circle

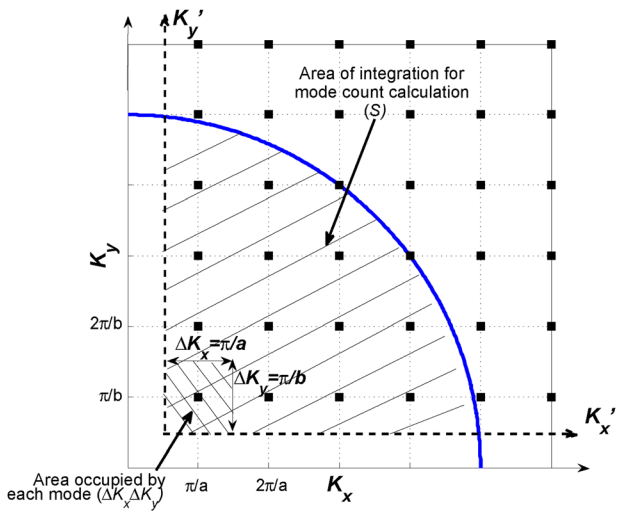

Fig. 2 Modes of a simply supported (SS–SS) flat plate shown in *k*-space

(Fig. 2). Accordingly, by differentiating Eqs. (14) and (15) with respect to frequency, the modal density is yield.

5 Mode Count and Modal Density of Circular Cylindrical Shells

In order to calculate the mode count and modal density of a cylindrical shell, the WSI method is introduced. First, the conventional WSI method proposed by previous researchers is studied. A MWSI technique is developed afterwards. This technique corrects the technical errors, which are present in the conventional method.

Comparing Eqs. (3) and (8), it is observed that unlike a flat plate, the k-plot of a shell is not a quarter circle. A more detailed analysis will prove that the 8th degree polynomial of Eq. (8) will have several unpredicted behaviors in the k-space. Thus, a closed form solution in the form of Eqs. (14) and (15) is not achievable for a cylindrical shell.

In Secs. 5 and 6, three shells with different geometries will be used to study the mode count and modal density of cylindrical shell structures. All these shells are made of aluminum with material properties; $E = 68.2\,\text{GPa}$, $\rho = 2700\,\text{kg/m}^3$, and $\upsilon = 0.33$. The geometrical characteristics of these shells are listed in Table 2. It is to note that in acoustical analysis, cylindrical shells are usually classified into two main groups [12] based on their mechanical and sound properties: (1) acoustically thick (if $(R/h) < 67$) and (2) acoustically thin (if $(R/h) > 67$). It is denoted that in Table 2 both acoustically thick and thin shells are depicted for evaluation generalization purposes.

5.1 Conventional WSI Method. In the conventional WSI, due to difficulties in integration of the 6th degree frequency equation (Eq. (6)), the simplified characteristic equation, Eq. (9) is used for integration in Eq. (13).

In Fig. 3, the modal curve of a simply supported cylindrical shell is plotted in the mn-space which is analogue to the k-space. The shell under consideration is shell no. 1 and the sample frequency is $\Omega = 0.1$ ($f = 1112\,\text{Hz}$). The formula used for determining the mode count is similar to Eq. (13), however, in the mn-space each mode occupies a 1×1 area. Thus, Eq. (13) is generalized for mn-space in the following form:

$$N(k) = \frac{\int_s dm \cdot dn}{1 \times 1} = \int_s dm \cdot dn \tag{16}$$

where S is again the area under the mode curve (Fig. 3). The area which is to be calculated according to the conventional WSI technique (Eq. (16)) is hatched in Fig. 3.

The above procedure is widely used in order to find the mode count and modal densities of circular cylindrical shells. Although, the conventional WSI is a straightforward and good technique, but the two main sources of error in this method are:

(1) The simplified characteristic equation (Eq. (9)) is used instead of the exact 6th degree equation (Eq. (6)). Since each mode is repeated at three distinct frequencies, using

Table 2 Shell dimensions under investigation (all dimensions are in meters)

Shell no.	Dimensions
1 (acoustically thick)	$h = 0.00147, R = 0.0762, l = 1.7272$; $R/h = 51.84, l/R = 22.67$
2 (acoustically thick)	$h = 0.0016, R = 0.0635, l = 0.2$; $R/h = 39.69, l/R = 3.15$
3 (acoustically thin)	$h = 0.003, R = 0.3, l = 1$; $R/h = 100, l/R = 3.33$

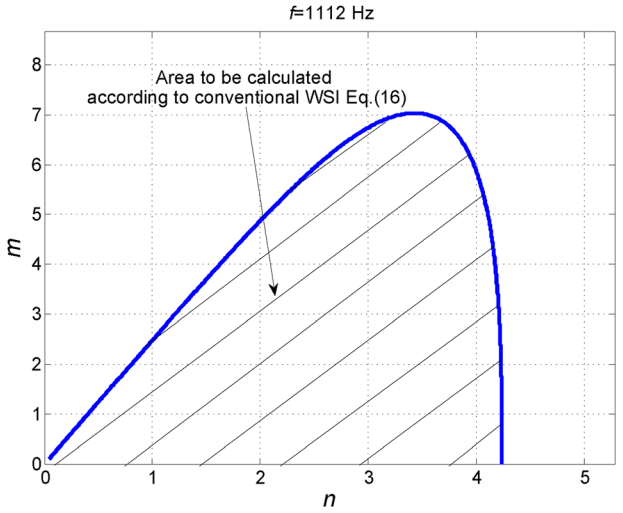

Fig. 3 Modes of a simply supported cylindrical (SS–SS) shell in the *mn*-space (analogue to *k*-space)

Eq. (9) as a simplified equation would omit two of the three frequencies. Thus, in the conventional WSI, many resonance modes are not taken into account due to simplifications in the characteristic equation.

(2) Independency of the mode count and modal density to boundary conditions is the second error in this technique. As observed by Fig. 3, there is no difference in the calculation of shells with different boundary conditions. Thus, according to this technique, the modal density and mode count are only functions of the shell's geometry and material properties. This is incorrect since it is obvious that shells with different boundaries possess different dynamic behaviors.

Due to these limitations, the conventional WSI method has not been used broadly in the SEA calculations. Consequently, in order to find acoustical properties in SEA analysis, alternative methods were applied instead of the WSI.

5.2 MWSI. As explained above, the conventional WSI consists of two major errors. In this section, a modified WSI method is proposed based on detailed analysis of the modal curves. The MWSI is applied to the exact 6th degree characteristic equation (Eq. (6)). Moreover, using a novel technique, the boundary effects are also exactly applied to final equations of the mode count and modal density. The MWSI technique is defined in two major steps that will correct the simplification and errors in the conventional method.

Step 1: Consider Eq. (6) as the exact characteristic equation. The *mn*-space of shell no. 1 according to Eq. (6) is plotted in Fig. 4 for three distinct frequencies: (a) low $\Omega_1 = 0.1$ ($F_1 = 1112$ Hz), (b) medium $\Omega_2 = 0.5$ ($F_2 = 5560$ Hz), and (c) high $\Omega_3 = 1.5$ ($F_3 = 16{,}680$ Hz). It is observed that at low frequencies ($\Omega_1 = 0.1$), the *mn*-space plot (Fig. 4(*a*)) is very similar to the plot with simplified equation (Fig. 3). At low frequencies similar to Fig. 3, the *mn*-space consists of only one curve; curve-1. Interestingly, as the frequency increases (Figs. 4(*b*) and 4(*c*)) instead of one curve (curve-1), the *mn*-space consists of two (curve-1 and curve-2) or three curves (curve-1, curve-2, and curve-3). Hence, it is clearly noticeable how Figs. 4(*b*) and 4(*c*) are conceptually different with Fig. 3.

Considering the explanation for mode repetition in cylindrical shells, these additional curves are fully understandable. As mentioned earlier, in cylindrical shells each pair of circumferential and axial wavenumbers (m and n) is repeated at three distinct frequencies. Each of these three resonance frequencies is associated with a primarily radial, axial or circumferential motion. Thus, the *mn*-space plot of a cylindrical shell versus frequency is actually a 3D plane, whereas the *mn*-space plotted for the mode count in the WSI method is a 2D plot. Therefore, the smaller curves (curve-1 and curve-2) observed in Figs. 4(*b*) and 4(*c*) are actual representations of the repeated mode shapes. Actually, in Fig. 4(*c*), the area under curve-2 (S_2) depicts the modes which are repeated for the second time and the area under curve-1 (S_1) depicts the modes which are repeated for the third time. Hence, the area below these additional smaller curves should be also calculated in order to find the exact mode count.

To understand this phenomena consider mode $(m, n) = \{(1, 0)\}$, which is repeated at three distinct frequencies; $f_1 = 892$ Hz, $f_2 = 1453$ Hz, and $f_3 = 11132$ Hz. This mode is illustrated in Fig. 4 by a black dot. Since f_1 is under $F_1 = 1120$ Hz, in Fig. 4(*a*) mode $(m, n) = \{(1, 0)\}$ is under the *mn*-space curve-1 and it is calculated in the mode count and integral of Eq. (16). Next, consider Fig. 4(*b*) in which both f_1 and f_2 are below $F_2 = 5560$ Hz, thus mode $(m, n) = \{(1, 0)\}$ is under curve-2 as well as curve-1. As a result, this mode should be integrated two times in Eq. (16). However, since the *mn*-space is a 2D diagram, $(m, n) = \{(1, 0)\}$ only occupies one point in the 2D-space and is only integrated once. Hence, it is not possible to calculate both of the $(m, n) = \{(1, 0)\}$ modes under the main curve and in a single integral. However, in Fig. 4(*b*), one could clearly see a second curve (curve-1) which is smaller. The modes below this smaller curve are actually the modes which are repeated for the second time similar to the $(m, n) = \{(1, 0)\}$ discussed above. Additionally, in Fig. 4(*c*), there is a curve-3 which is larger than curve-1 and curve-2. In Fig. 4(*c*), the modes under curve-1 represent the third and final resonance frequencies (f_3 in this case which is below $F_3 = 16{,}680$ Hz). In conclusion, in order to find the exact mode count, the areas below all the three curves should be taken into account and integrated.

In Fig. 5, repetition of modes is identified by different markers. Modes which are repeated for one, two, and three times are marked by "•," "○," and "*," respectively. Clearly, the repetition of each mode is classified by the three frequency curves in the *mn*-space, which is only obtained by using the exact characteristic equation, Eq. (6).

Thus, the repetition of modes should be considered when integrating in the *mn*-space. According to the MWSI, Eq. (16) should be corrected in the following form:

$$N(k) = \int_{S_1} dm \cdot dn + \int_{S_2} dm \cdot dn + \int_{S_3} dm \cdot dn \qquad (17)$$

in which S_1, S_2, and S_3 are the areas under curve-1, curve-2, and curve-3, respectively. Accordingly, at low frequencies, $S_2 = S_3 = 0$, whereas, at higher frequencies due to repetitions of modes: $S_2 \neq 0$ and/or $S_3 \neq 0$. Therefore, the first step in the MWSI method is to determine and evaluate the three integrals of Eq. (17).

Step 2: Now, let us explain the effects of boundary conditions in this method. Consider Table 1 in which $m = 1, 2, 3, \ldots$ and $n = 0, 1, 2, \ldots$. In this section, the effects of SS–SS and C–C boundary conditions will be studied on the modal distribution of cylindrical shells.

(a) Simply supported cylindrical shell
For a simply supported boundary condition, since $k_a = (m\pi/l)$, the complete k-space plot and modes, which should be calculated in the integral of Eq. (17) are shown in Fig. 6. For cylindrical shells, each mode in the k-space occupies a space of $(\pi/l) \times (1/R)$. By representing each mode with a square of dimensions $(\pi/l) \times (1/R)$, only the modes present in the hatched areas of Fig. 6 should be accounted in Eq. (17). Thus, for a simply supported shell, a half strip along the y-axis with a width of $(1/2R)$ should be included, whereas a half strip along the x-axis with a width of $(\pi/2l)$ should be deducted. These additions and

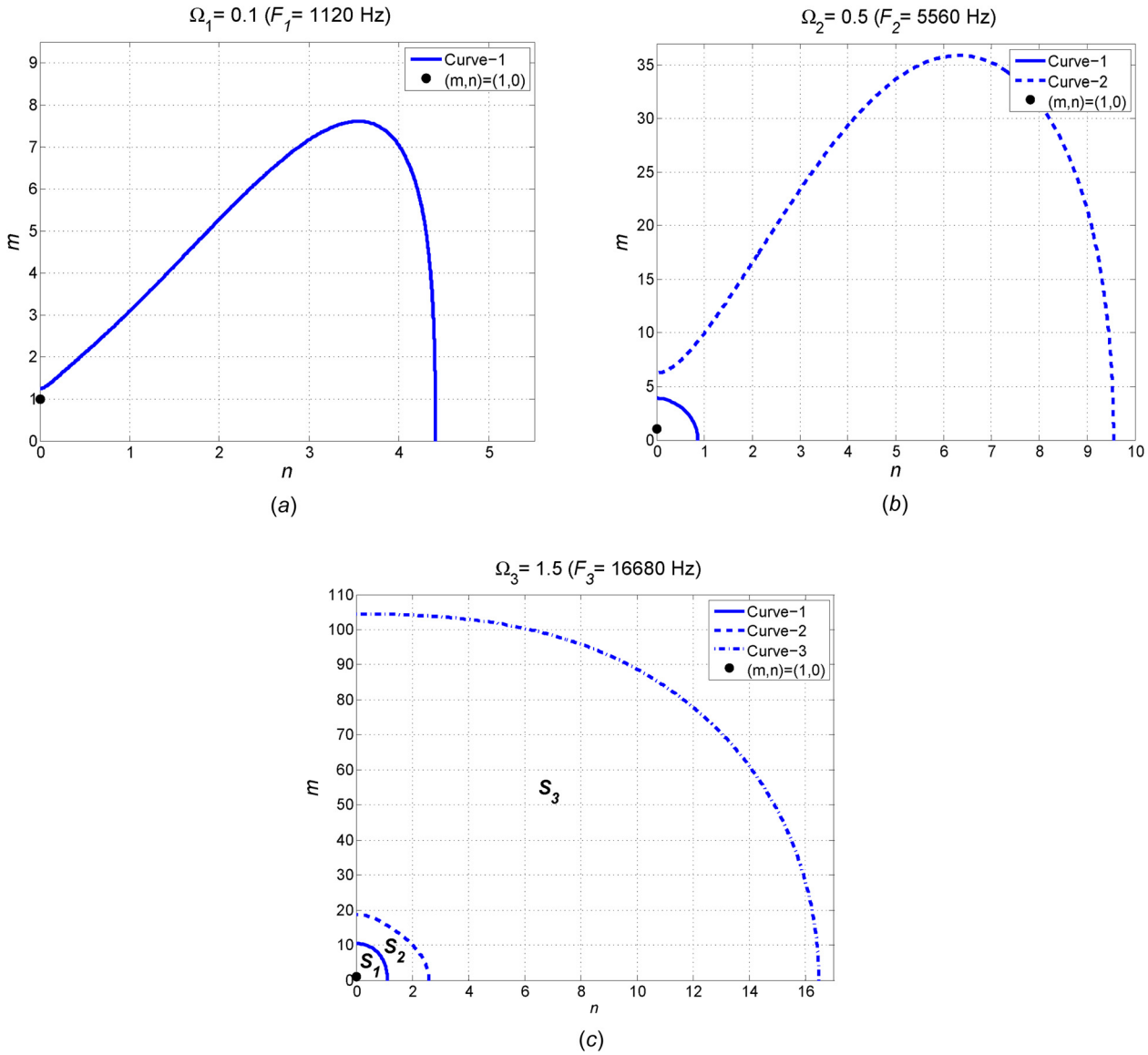

Fig. 4 Modal plot of shell no. 1 in the *mn*-space: (*a*) low frequency $\Omega_1 = 0.1$ ($F_1 = 1112$ Hz), (*b*) medium frequency $\Omega_2 = 0.5$ ($F_2 = 5560$ Hz), and (*c*) high frequency $\Omega_3 = 1.5$ ($F_3 = 16680$ Hz)

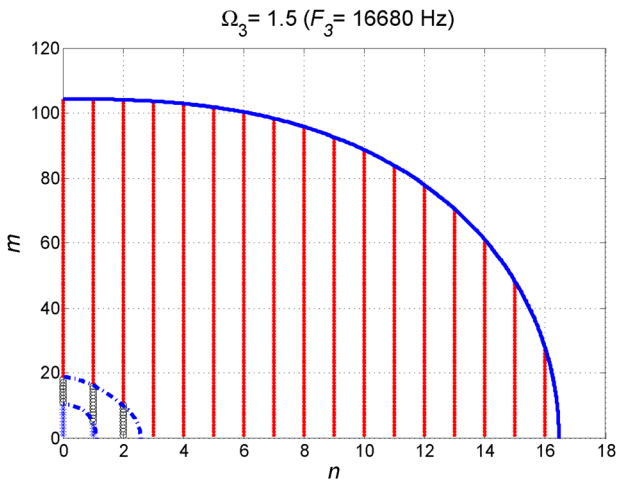

Fig. 5 Mode repetition identified by different markers: (1) once "●," (2) twice "○," and (3) trice "*" repeated modes

subtractions are due to axial and circumferential wavenumbers m and n, which start from 1 and 0, respectively. In general, such additions and subtractions can be achieved by transferring the k_a and k_c axes and calculating Eq. (17) in the new transferred axes $k'_a - k'_c$ which are shown in Fig. 6. Considering definitions of $k_a = (m\pi/l)$ and $k_c = (n/R)$ such transformation is applied through the following transformation of the *mn*-axes:

$$\begin{cases} m = m' + \dfrac{1}{2} \text{ results in addition of the } \dfrac{\pi}{2l} \text{ strip} \\ n = n' - \dfrac{1}{2} \text{ results in subtraction of the } \dfrac{1}{2R} \text{ strip} \end{cases} \tag{18}$$

in which m' and n' are the new transferred axes. Therefore, for a SS–SS cylindrical shell, the mode count (Eq. (17)) should be calculated in the transferred $m'n'$-space defined by Eq. (18) rather than the *mn*-space.

(b) Clamped cylindrical shell

Next, consider a shell with C–C boundary conditions in which; $k_a = (2(m+1)\pi/l)$. The *k*-space of a clamped shell is shown in Fig. 7. Although, similar to the simply

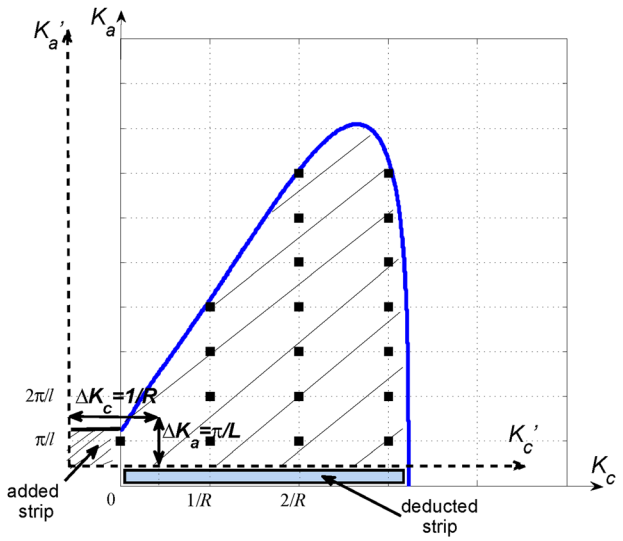

Fig. 6 Modes of a simply supported (SS–SS) circular cylindrical shell shown in *k*-space; added half strip (hatch area) and deducted half strip (box)

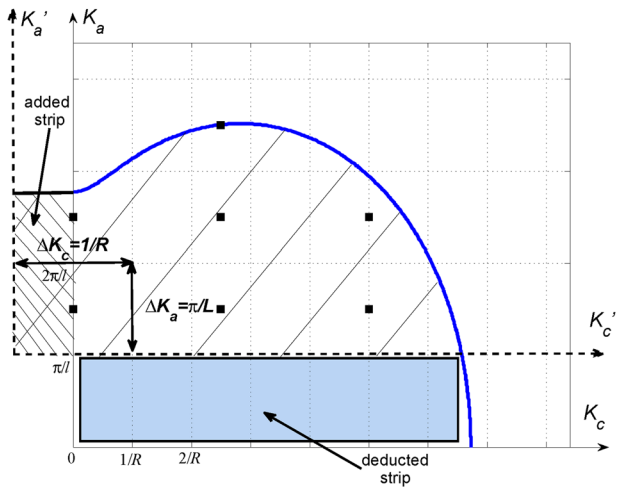

Fig. 7 Modes of a clamped (C–C) circular cylindrical shell shown in *k*-space; added half strip (hatched area) and deducted full strip (box)

supported condition, a half strip should be subtracted along the x-axis, but a different result is obtained along the y-axis. In the clamped case, the width of the subtracted strip along the y-axis is (π/l). This is because the clamped and simply supported shells have different axial wave parameters (Table 1), whereas their circumferential wave parameters are the same. Similar to Eq. (18), for a clamped cylindrical shell, the below transformations should be applied in the mn-space

$$\begin{cases} m = m' + 1 \text{ results in addition of the } \dfrac{\pi}{l}\text{strip} \\ n = n' - \dfrac{1}{2} \text{ results in subtraction of the } \dfrac{1}{2R} \text{ strip} \end{cases} \tag{19}$$

Consequently, for a C–C cylindrical shell, the mode count (Eq. (17)) should be integrated in the $m'n'$-space defined by Eq. (19) rather than the original mn-space.

As observed in Figs. 6 and 7, a novel technique is introduced in the MWSI so one could apply the effects of boundary conditions in the mn-space. By considering the wave parameters for different boundary conditions (Table 1), different transformations are resulted for m' and n'.

To conclude the remarks made above, the final mode count function according to the MWSI method should be written as follows:

$$N(k) = \int_{S_1} dm' \cdot dn' + \int_{S_2} dm' \cdot dn' + \int_{S_3} dm' \cdot dn' \tag{20}$$

where m' is the transformation of m and n' is the transformation of n according to any specific boundary condition. The final formulation of the MWSI technique is obtained through Eq. (20) in which the two steps are summarized as follows:

(1) Step 1: Three mode curves should be integrated in the $m'n'$-space since each curve represents a repetition of the modes underneath.
(2) Step 2: The modal curves should be integrated in a transferred $m'n'$-space which is a transformation of the mn-space and varies for each boundary condition (Eq. (18) for SS–SS and Eq. (19) for C–C boundary conditions).

6 Discussion

6.1 Verification of MWSI Method. The modified wave number space integration method was explained in two steps. Each step is a correction to the errors present in the conventional WSI. In this section, mode counts and modal densities are obtained according to four different methods: (1) exact numerical mode count (step function), (2) conventional WSI (Eq. (16)), (3) MWSI without boundary condition (BC) effects (MWSI w/o BC) (Eq. (17)), and (4) MWSI with BC effects (MWSI w BC) (Eq. (20)). The aim is to compare results of the MWSI and conventional WSI with the exact number of mode count obtained from numerical calculation to investigate the accuracy of the proposed technique.

In Tables 3–8, mode counts have been calculated for the three shells of different geometries for two boundary conditions: (a) simply supported (SS–SS) and (b) clamped (C–C).

Tables 3 and 4 represent mode counts of shell no. 1, which is a long acoustically thick shell with small geometrical thickness. It is clear that for an SS–SS shell (Table 3) the WSI yields the highest errors in all frequency ranges. Errors of the WSI decrease at high frequencies; nevertheless, even at high frequencies, this theory underestimates over 100 modes, which is a crucial error. Both the MWSI techniques with and without BC effects predict the mode count with great accuracy. Moreover, it is clearly evident that MWSI w BC, Eq. (20), is much more accurate compared

Table 3 Mode count of shell no. 1 for SS–SS boundary conditions

	0.1		0.5		1		1.5		2	
Nondimensional frequency	Mode count	Error	Mode count	Error (%)	Mode count	Error (%)	Mode count	Error (&)	Mode count	Error (%)
Exact	23	—	241	—	847	—	1514	—	2102	—
WSI (Eq. (16))	18.7	18.70	225.4	6.473	796.46	5.97	1403.1	7.32	1946.3	7.41
MWSI w/o BC (Eq. (17))	22.4	2.61	241.3	0.12	819.46	3.25	1455.5	3.86	2038.5	3.02
MWSI w BC (Eq. (20))	20.7	10.00	240.7	0.12	845.12	0.22	1511.2	0.18	2109.2	0.34

Table 4 Mode count of shell no. 1 for C–C boundary conditions

	0.1		0.5		1		1.5		2	
Nondimensional frequency	Mode count	Error	Mode count	Error (%)	Mode count	Error (%)	Mode count	Error (&)	Mode count	Error (%)
Exact	18	—	236	—	840	—	1504	—	2088	—
WSI (Eq. (16))	16.63	7.61	220.69	6.49	789.85	5.97	1394.9	7.25	1936.8	7.24
MWSI w/o BC (Eq. (17))	20.12	11.78	236.10	0.04	811.87	3.35	1445.5	3.89	2026.4	2.95
MWSI w BC (Eq. (20))	15.81	12.17	229.36	2.81	828.96	1.31	1489.6	0.96	2083.6	0.21

Table 5 Mode count of shell no. 2 for SS–SS boundary conditions

	0.1		0.5		1		1.5		2	
Nondimensional frequency	Mode count	Error	Mode count	Error (%)	Mode count	Error (%)	Mode count	Error (&)	Mode count	Error (%)
Exact	—	—	22	—	85	—	155	—	219	—
WSI (Eq. (16))	—	—	23.98	9.00	84.7	0.35	149.2	3.74	207.05	5.46
MWSI w/o BC (Eq. (17))	—	—	26.14	18.82	87.93	3.45	156.57	1.01	219.88	0.40
MWSI w BC (Eq. (20))	—	—	21.82	0.82	84.9	0.12	155.18	0.12	218.75	0.11

Table 6 Mode count of shell no. 2 for C–C boundary conditions

	0.1		0.5		1		1.5		2	
Nondimensional frequency	Mode count	Error	Mode count	Error (%)	Mode count	Error (%)	Mode count	Error (&)	Mode count	Error (%)
Exact	—	—	16	—	79.00	—	146	—	208	—
WSI (Eq. (16))	—	—	19.96	24.75	78.87	0.16	142.00	2.74	198.77	4.44
MWSI w/o BC (Eq. (17))	—	—	21.6	35.00	81.20	2.78	147.53	1.05	208.99	0.48
MWSI w BC (Eq. (20))	—	—	13.72	14.25	71.16	9.92	136.28	6.66	195.92	5.81

Table 7 Mode count of shell no. 3 for SS–SS boundary conditions

	0.1		0.5		1		1.5		2	
Nondimensional frequency	Mode count	Error	Mode count	Error (%)	Mode count	Error (%)	Mode count	Error (&)	Mode count	Error (%)
Exact	3	—	61	—	224	—	405	—	565	—
WSI (Eq. (16))	5.31	77.00	63.95	4.84	225.95	0.87	398.04	1.72	552.15	2.27
MWSI w/o BC (Eq. (17))	5.89	96.33	66.41	8.87	229.32	2.38	405.93	0.23	565.67	0.12
MWSI w BC (Eq. (20))	3.06	2.00	59.70	2.13	225.19	0.53	404.5	0.12	565.14	0.02

Table 8 Mode count of shell no. 3 for C–C boundary conditions

	0.1		0.5		1		1.5		2	
Nondimensional frequency	Mode count	Error	Mode count	Error (%)	Mode count	Error (%)	Mode count	Error (&)	Mode count	Error (%)
Exact	—	—	50	—	214	—	388	—	550	—
WSI (Eq. (16))	—	—	57.48	14.96	216.65	1.24	386.64	0.35	538.99	2.00
MWSI w/o BC (Eq. (17))	—	—	59.45	18.90	219.15	2.40	392.49	1.16	549.92	0.01
MWSI w BC (Eq. (20))	—	—	52.85	5.70	214.67	0.31	377.09	2.81	532.53	3.18

to MWSI w/o BC, Eq. (17), except at $\Omega = 0.1$ which is low frequency. It is very interesting that the MWSI predicts the mode count with nearly no errors, which is remarkable compared to all other WSI techniques present in literature.

In Table 4, mode counts are calculated for shell no. 1, however, with clamped boundary conditions. Similar to the SS–SS boundary conditions, WSI (Eq. (16)) yields the highest errors, whereas both the MWSI techniques yield smaller errors. Interestingly, MWSI w BC effects is much more accurate compared to MWSI w/o BC effects.

Tables 5 and 6 represents mode counts of shell no. 2 which is a short acoustically thin shell with small geometrical thickness. Results are very similar to Tables 3 and 4. However, for such a short shell with SS–SS boundary conditions, the MWSI w BC effects (Eq. (20)) is also accurate at low frequencies. Moreover, for the C–C boundary at low frequencies, all techniques yield high errors except Eq. (20).

Tables 7 and 8 represent mode counts of shell no. 3 which is a short acoustically thin shell, with a large geometrical thickness. For the SS–SS case (Table 7), Eq. (20) obtained very accurate

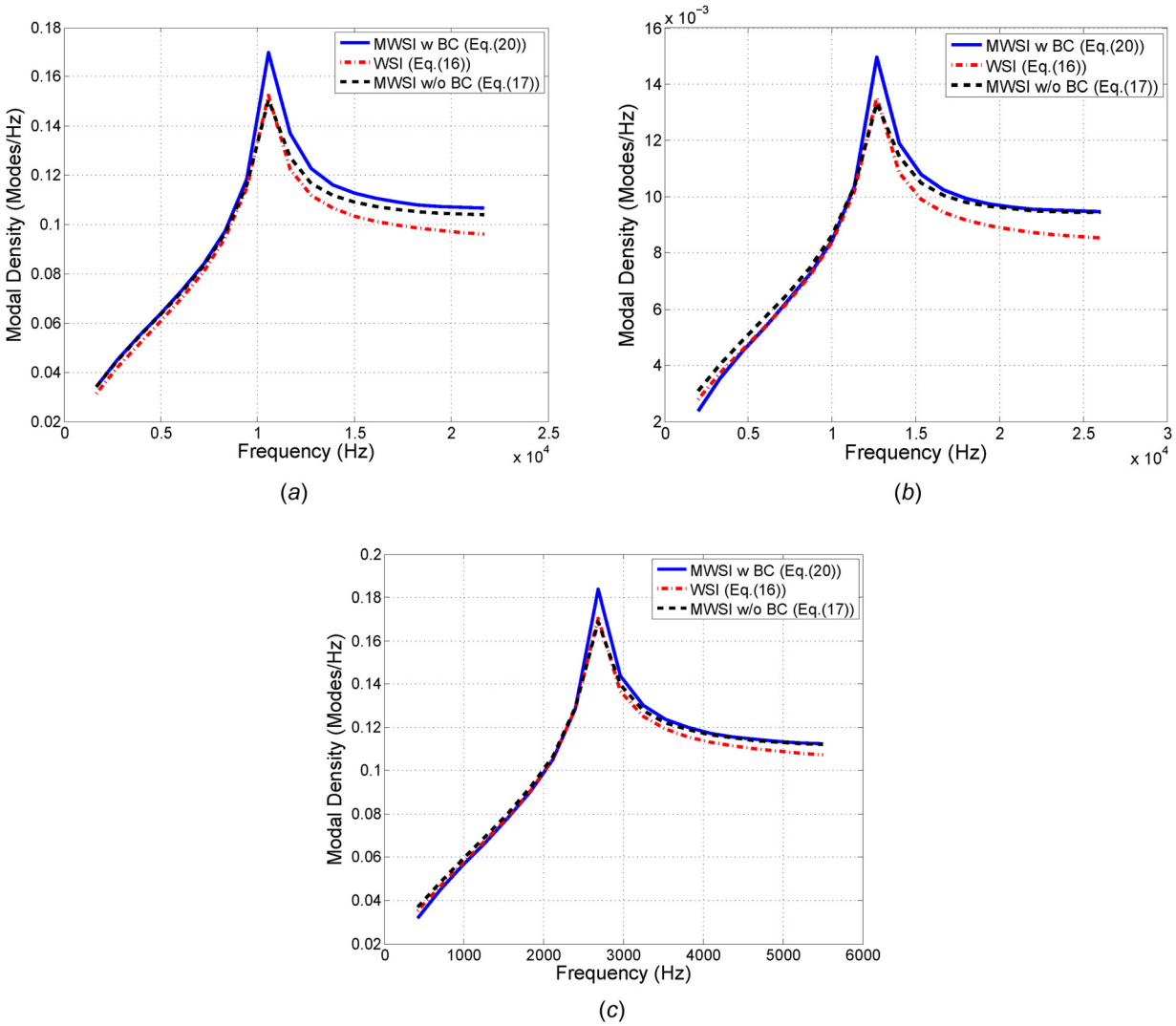

Fig. 8 Modal densities of the three shells according to different theories: (*a*) shell no. 1, (*b*) shell no. 2, and (*c*) shell no. 3

results. This is specially observed at $\Omega = 0.1$, in which both Eqs. (16) and (17) yield errors of higher than 60%, whereas Eq. (20) has an error of only 2%. Thus, the effect of boundary conditions on mode count calculation is clearly observed in this case.

Reviewing Tables 3–8, it is clearly observed that the MWSI method with boundary conditions Eq. (20) is the most accurate method amongst all other methods for both SS–SS and C–C boundary conditions. The conventional WSI did not obtain accurate results especially at low frequency, whereas the MWSI method was accurate for all frequency ranges. In addition, Eq. (17), which is a more simplified version of the MWSI without the effects of boundary conditions, also yields reasonable solutions. As a result, it is recommended to use the MWSI method, Eq. (20), instead of the conventional WSI, Eq. (16), in order to estimate mode count and modal densities of cylindrical shells.

In Fig. 8, modal densities have been calculated for the three shells according to all theories discussed above. It is clear from Fig. 8 that the modal densities of all cylindrical shells have a similar general trend. At first, the modal density increases with a constant slope until it reaches a maximum at the ring frequency. At the ring frequency, several resonance modes are closely spaced in a short frequency band, thus producing a large modal density. Beyond the ring frequency, the modal density decreases into a constant value behaving more like a flat plate.

In Fig. 8(*a*), which is for shell no. 1 (acoustically thick and geometrically long and thin), the MWSI w BC effects yields the higher bound for the modal density at all frequencies. On the other hand, the WSI results in a lower bound which is a result of miscalculation of modes as stated previously (Table 3). Such underestimation of the mode count in the WSI is more clear after the ring frequency. The MWSI w/o BC effects is an average of the two other methods, predicting a modal density in between the upper and lower bounds. However, at the ring frequency, their results are closer to the WSI.

The modal density of the short acoustically thin shell with small thickness is illustrated in Fig. 8(*b*). Results are quite different compared to Fig. 8(*a*). In Fig. 8(*b*), the MWSI w BC effects does not always yield the higher bound for the modal density. Before the ring frequency, both the WSI and MWSI w/o BC effects yield higher modal densities compared with the MWSI w BC effects, whereas at the ring frequency and above, both methods yield lower amounts. Figure 8(*c*) is the modal density plot for the short acoustically thin shell with a high thickness. The trend is very similar to Fig. 8(*b*).

Comparing modal densities of the three shells, it is interesting that the modal density for shell no. 2 (Fig. 8(*b*)) is an order of magnitude smaller compared to shell nos. 1 and 3. Therefore, resonance frequencies are spaced further apart from each other. This is mainly due to the low thickness (R/h) and aspect ratio (l/R) of shell no. 2 which makes it harder for structure wavelengths to couple and produce large distortions in the shell. Thus, reducing the number of resonance frequencies in the shell.

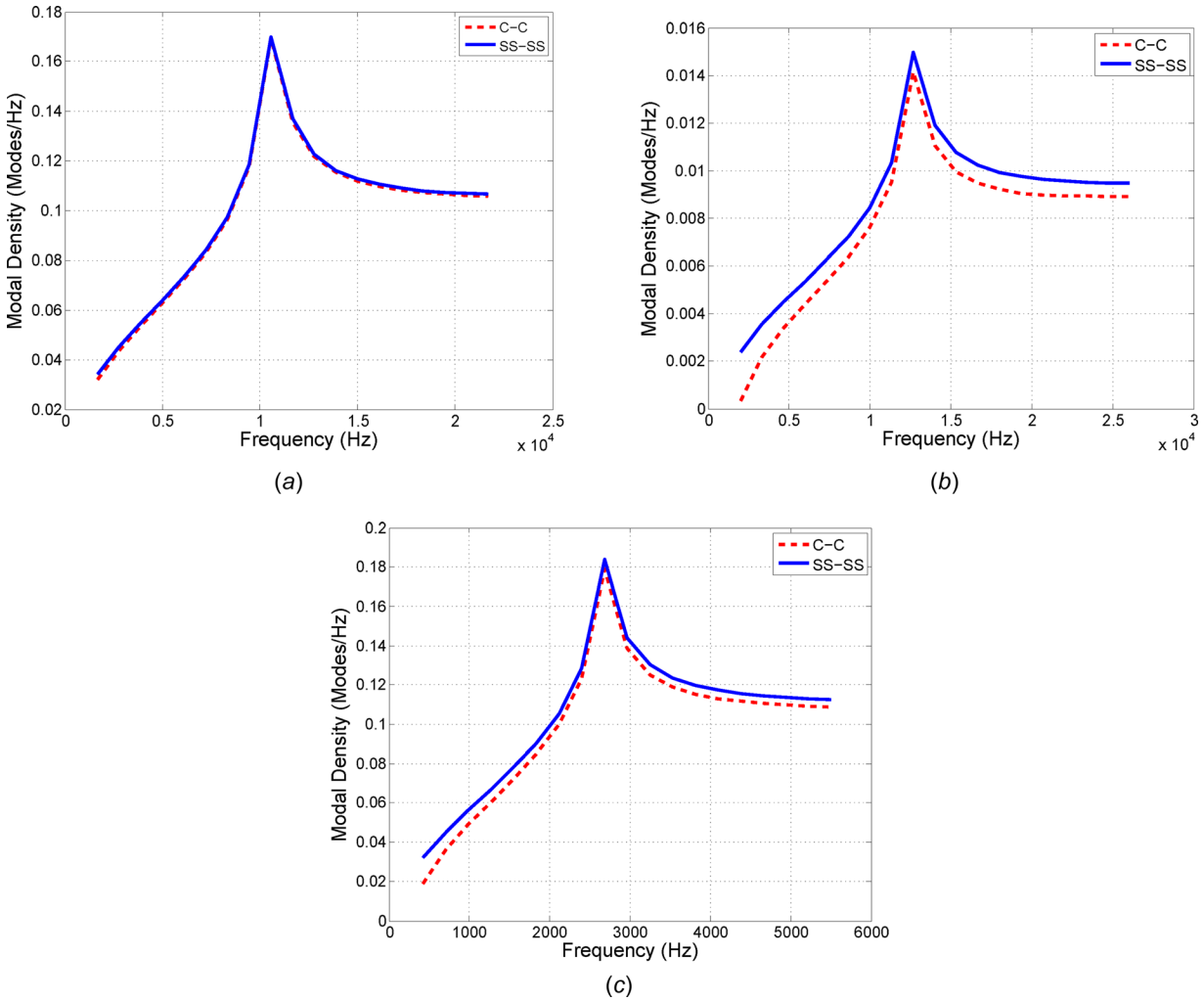

Fig. 9 Modal densities of the three shells for simply supported (SS–SS) and clamped (C–C) boundary conditions: (*a*) shell no. 1, (*b*) shell no. 2, and (*c*) shell no. 3

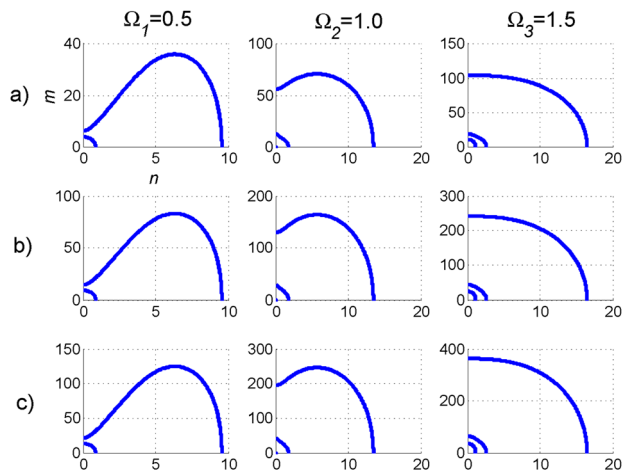

Fig. 10 Modification of mode plots with length variation in *mn*-space: (*a*) $l = 1.73$ m, (*b*) $l = 4$ m, and (*c*) $l = 6$ m (each column is obtained for a similar frequency and each row is for a fixed shell length)

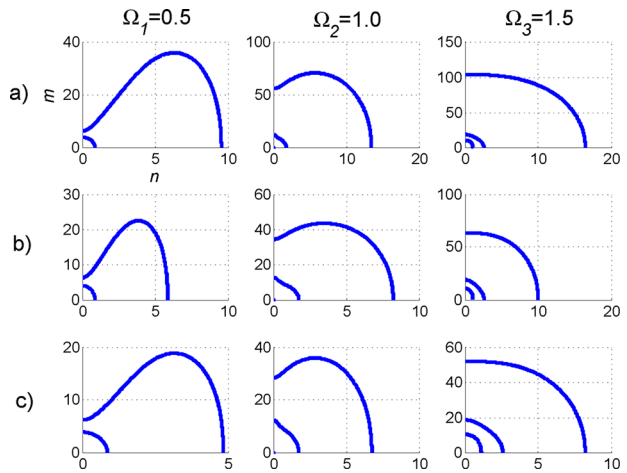

Fig. 11 Modification of mode plots with thickness variation in *mn*-space: (*a*) $h = 0.00147$ m, (*b*) $h = 0.004$ m, and (*c*) $h = 0.006$ m (each column is obtained for a similar frequency and each row is for a fixed shell length)

As stated earlier, one of the main advantages of the MWSI technique is the contribution of BC effects in the *k*-space which is applied through step 2 of the technique. It was observed in Tables 3–8 that shells with different boundary conditions yield different mode counts. Now let us analyze modal densities of shells with different boundary conditions. In Fig. 9, modal densities of the three shells are plotted for simply supported (SS–SS) and clamped (C–C) boundary conditions. According to Fig. 9(*a*), the clamped

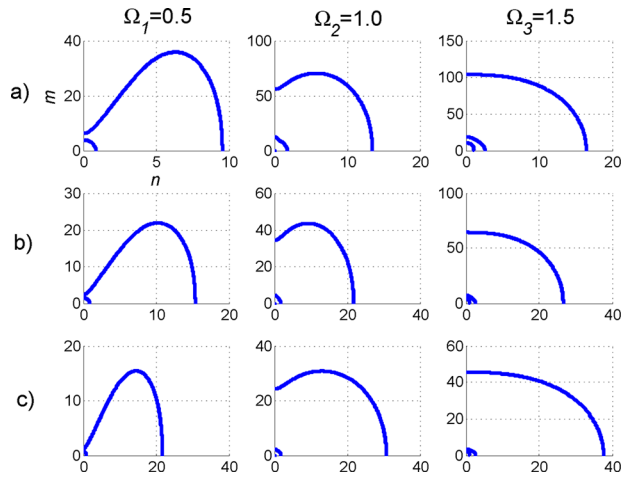

Fig. 12 Modification of mode plots with radius variation in *mn*-space: (*a*) $R = 0.0762$ m, (*b*) $R = 0.2$ m, and (*c*) $R = 0.4$ m (each column is obtained for a similar frequency and each row is for a fixed shell length)

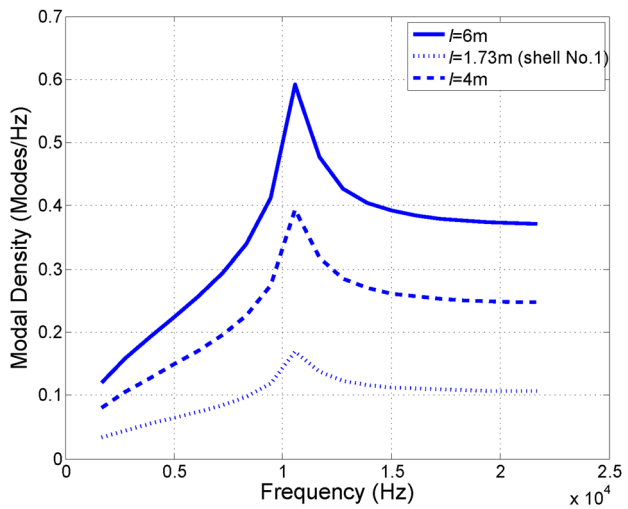

Fig. 13 Modal densities of shells with different lengths

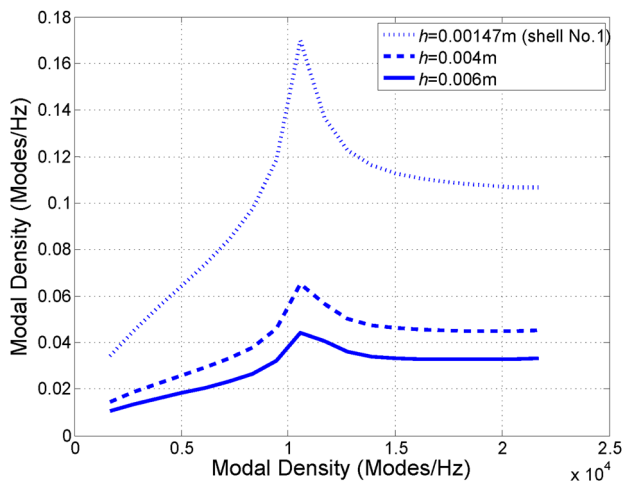

Fig. 14 Modal densities of shells with different thicknesses

and simply supported boundary conditions of shell no. 1 are not much different in terms of modal density. However, this is not the case for shell nos. 2 and 3. In Fig. 9(*b*), it is observed that the modal density in C–C boundary conditions is 0.001 (modes/Hz)

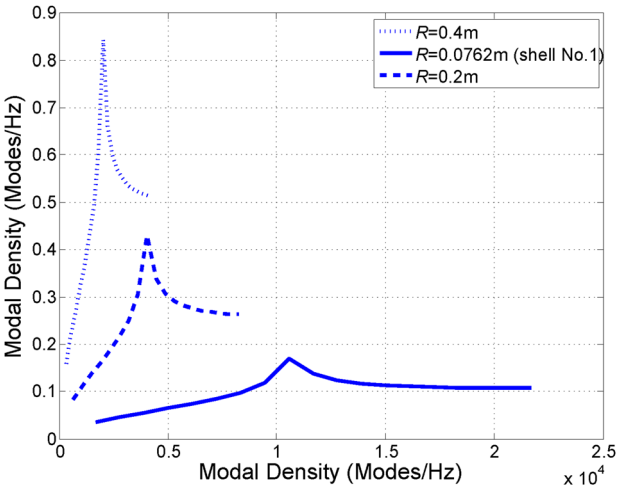

Fig. 15 Modal densities of shells with different radii

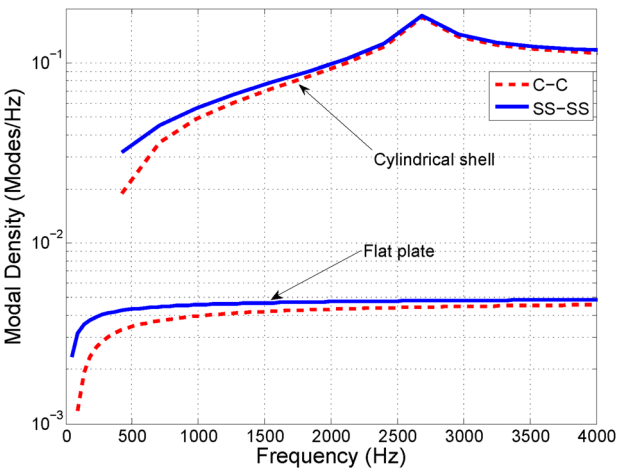

Fig. 16 Modal density of a cylindrical shell compared to a flat plate at two different boundary conditions

less than the SS–SS case, whereas this difference is less for shell no. 3 (Fig. 9(*c*)). Thus, it is clearly evident that the modal density is dependent on boundary conditions. However, the degree of this dependency on the final result is dependent on the shells' geometrical and mechanical properties.

6.2 Effects of Geometrical Properties on Mode Plots and Modal Density. In Figs. 10–12, the contribution of shell geometrical properties (length, radius and thickness) is studied on the mode count plots. In Fig. 10, mode plots are obtained at three non-dimensional frequencies for three shells of different lengths but similar geometries. The characteristic equation is plotted in the *mn*-space (wavenumber space) as a function of *m* (axial wavenumber) and *n* (circumferential wavenumber) to analyze the effects of length variation on modal distribution. It is obvious from Fig. 10 that the change of length does not change the shape of the modal curve; however, it does change the mode shapes and values of the mode count curves. The maximum axial waveparameter *m* of the mode count plots increases with increasing length. On the other hand, the maximum circumferential waveparameter *n* remains the same at all lengths. This predicts a higher mode count for longer shells. In conclusion, for long cylindrical shells, the axial waveparameter plays a more crucial role in the modal analysis. This is due to the fact that the mode shapes possess higher numbers of *m* at longer lengths.

In Fig. 11, the effects of shell thickness are evaluated on the mode count of cylindrical shells. As the thickness increases, both

axial and circumferential waveparameters of the main curve decrease, denoting lower mode shapes and resonance frequencies. Such behavior signifies a harder excitation for thick shells. Conversely, for the second and third modal curves, which represent repeated modes, there are no changes with thickness at all. More importantly, in all three frequencies, the gap between the main and second modal curves decreases with increasing thickness. Thus, with the second curve remaining constant and the main curve decreasing a larger percentage of mode shapes are repeated for thick cylindrical shells.

In Fig. 12, curves are plotted for shells of different radii in the *mn*-space. Since the radius has a direct effect in the nondimensional frequency (Eq. (7)), the actual frequency in Hz is different for the three shells. Generally, as the radius increases, the frequency in Hz decreases, although Ω is the same. Frequency in Hz decreases for larger radius, whereas the maximum circumferential waveparameter n increases with increasing radius. On the other hand, the axial waveparameter decreases with increasing radius, which is credited to the decreasing frequency. As a result, in shells with larger radius circumferential waveparameter is of more importance and the mode shapes obtain larger numbers of n. Moreover, the second and third curves seem to shrink with increasing radius. This should again be credited to the decreasing frequency in Hz, which defines lower percentage of repeated modes. However, when modal curves were plotted for the three shells at same frequencies in Hz, third modal curves (third repetitions) were noticed for larger radius, whereas the smaller radius were still only in their second repetition modes. Thus, one could clearly conclude that as the radius increases there is a higher chance that the mode shapes will be repeated.

In Figs. 13–15, modal densities are calculated for shells of different lengths, thicknesses, and radii. As illustrated in Fig. 13, the modal density is directly proportional to the length. This was also anticipated from the modal curves in *mn*-space (Fig. 12) where the maximum axial waveparameter increased with length. On the other hand, Fig. 14 implies that the modal density is inversely proportional to thickness. This is also explainable from the *mn*-curves in Fig. 11. Since the radius of the main modal curve decreased with increasing thickness there would be fewer modes available under the modal curve. This would also result in modes being spaced further apart. Finally, Fig. 15 represents variation of modal density with radius. This modal density curve (Fig. 15) is totally different compared to the two previous cases (Figs. 13 and 14). By increasing the radius, ring frequency of the shell decreases. Thus, the shell with the smallest radius reaches its modal density peak at a smaller ring frequency. More importantly, with increasing the shell radius the modal density values increases likewise over all frequency ranges.

6.3 Cylindrical Shell and Plate Modal Density Comparison. Finally, in Fig. 16, modal densities of shell no. 3 are compared to a flat plate with similar boundary conditions and geometry. It is interesting that unlike a cylindrical shell modal density of a flat plate increases until it reaches an asymptote. There are no modal density peaks for the flat plate. The modal density is increased dramatically as the flat plate is curved into a cylindrical shell. The constant modal density of the shell after the ring frequency is nearly 20 times higher than the flat plate. This ratio was found to be different for the other two shells. The ratio of the shell modal density after the ring frequency to the plate for shell nos. 1 and 2 were 10 and 50, respectively. Therefore, there is no constant value for modal density ratio of a flat plate to a cylindrical shell. Similarly, this ratio is also completely dependent on the shell's geometry and mechanical properties.

7 Conclusion

Mode count and modal densities of circular cylindrical shells were obtained by a MWSI method. The conventional WSI was presented and the drawbacks of the method were identified. An MWSI method was presented in two separate steps. In the first step, the exact equation of motion was substituted with the simplified version. Results showed that instead of only one modal curve there exist two or three modal curves. Each of these extra modal curves is a representation of the repeated modes in cylindrical shells. In the second step, a novel technique was applied in order to introduce the effects of boundary conditions to the MWSI method. A final modified formula was obtained for the MWSI method by integrating observations in both steps.

Three shells of different geometrical and acoustical properties were identified for evaluation of the MWSI method. Comparing results of exact mode count calculations with MWSI and WSI methods, it was revealed that the MWSI method was by far more accurate than the conventional WSI. Modal densities were obtained comparing the MWSI and WSI methods. Generally, the modal density of a cylindrical shell increased up to the ring frequency. At the ring frequency, a large number of modes were closely spaced together producing a peak in the modal density plot. Beyond the ring frequency the modal density relaxed into a constant value. Compared to MWSI, the WSI underestimated modal density for some shells and overestimated for others. However, this trend is understandable if the shells were to be classified as acoustically thick and thin. Modal densities were also obtained with and without boundary condition effects. Previous researchers did not include the effects of boundary conditions, whereas it was observed that boundary conditions were in fact influential on the mode count and modal density calculations. Although the conventional WSI is inaccurate in most cases, the degree of this inaccuracy decreases when the boundary conditions have a minor effect (e.g., the case of long and thin cylinders). Hence, the conventional WSI may be applicable to some certain cases considering the amount of accuracy required.

Length, radius, and thickness variations were studied on the mode count plots using the MWSI method. It was observed that in shells of larger thickness and radius a higher percentage of modes were repeated. Effects of shell geometrical properties were also studied on modal density. For shells of larger radius since the ring frequency is decreased, the modal density peak occurred at a lower frequency. Finally, modal densities of plates and shells were compared. Results of this technique (MWSI) will be very beneficial in sound transmission and sound radiation analysis of circular cylindrical shells in which the modal density calculations play an important role.

Nomenclature

A, B, C = modal (wave) amplitudes in axial, circumferential, and radial directions, respectively
D = bending stiffness of a flat plate
E = Young's modulus of elasticity
f_r = ring frequency
h = shell thickness
k_a = axial wavenumber of a cylindrical shell
K_i $(i = 1, 2, 3, 4)$ = real parts of characteristic equation roots
k_x = wavenumber of a flat plate in x-direction
k_y = wavenumber of a flat plate in y-direction
l = shell length
L_i $(i = 1,\ldots, 6)$ = partial differential operators
m = longitudinal wave parameter
M = mass per unit area of a flat plate
m' = transferred axes of the longitudinal wave parameter
n = circumferential wave parameter
n' = transferred axes of the circumferential wave parameter
$n(k)$ = modal density
$N(k)$ = average mode count
p_i $(i = 2, 4, 6)$ = coefficients of Flugge characteristic equation
q_i $(i = 0, 2, 4, 6)$ = coefficients of characteristic equation
R = shell radius

u, v, w = axial, circumferential, and radial components of displacement, respectively
W = out of plane displacement of a flat plate
x = longitudinal coordinate of shell/plate
y = horizontal coordinate of plate
β = nondimensional thickness parameter
η = normal mode count
θ = circumferential coordinate of shell
λ = wavelength of sound wave
ρ = mass density
υ = Poisson's ratio
ω = circular natural frequency
Ω = nondimensional frequency parameter

Appendix

Differential Operators L_{ij}. According to the Flugge Theory (Eq. (4))

$$L_{11} = R^2\frac{\partial^2}{\partial x^2} + (1+\beta)\frac{(1-\upsilon)}{2}\frac{\partial^2}{\partial\theta^2} - \frac{\rho h R^2}{B}\frac{\partial^2}{\partial t^2}$$

$$L_{13} = \upsilon R\frac{\partial}{\partial x} - R^3\beta\frac{\partial^2}{\partial x^3} + \frac{(1-\upsilon)}{2}R\beta\frac{\partial^3}{\partial x\partial\theta^2},\quad L_{12} = \frac{1+\upsilon}{2}R\frac{\partial^2}{\partial x\partial\theta},$$

$$L_{21} = L_{12}$$

$$L_{22} = \left[\frac{1-\upsilon}{2}R^2 + \frac{3}{2}(1-\upsilon)R^2\beta\right]\frac{\partial^2}{\partial x^2} + \frac{\partial^2}{\partial\theta^2} - \frac{\rho h R^2}{B}\frac{\partial^2}{\partial t^2},$$

$$L_{23} = -\frac{(3-\upsilon)}{2}R^2\beta\frac{\partial^3}{\partial x^2\partial\theta} + \frac{\partial}{\partial\theta}$$

$$L_{31} = L_{13},\quad L_{32} = L_{23}$$

$$L_{33} = 1 + \left(1 + \nabla^4 + 2\frac{\partial^2}{\partial\theta^2}\right)\beta + \frac{(1-\upsilon^2)\rho R^2}{E}\frac{\partial^2}{\partial t^2}$$

$$D = \frac{Eh}{1-\upsilon^2},\quad \beta = \frac{h^2}{12R^2}$$

Coefficients of Characteristic Equation. For Flugge Characteristic Equation (Eq. (6))

$$p_4 = 1 + \frac{1}{2}(3-\upsilon)(n^2+k_a^2) + \beta(n^2+k_a^2)^2$$

$$p_2 = \frac{1}{2}(1-\upsilon)\left[(3+2\upsilon)k_a^2 + n^2 + (n^2+k_a^2)^2 + \frac{(3-\upsilon)}{(1-\upsilon)}\beta(n^2+k_a^2)^3\right]$$

$$p_0 = \frac{1}{2}(1-\upsilon)\left[(1-\upsilon^2)k_a^4 + +\beta(n^2+k_a^2)^4\right] + \frac{\beta}{2}(1-\upsilon)\begin{bmatrix}2(2-\upsilon)k_a^2n^2 + n^4 - 2\upsilon k_a^6 - 6k_a^4n^2\\ -(4-\upsilon)k_a^2n^4 - 2n^6\end{bmatrix}$$

References

[1] Maa, D. Y., 1939, "Distribution of Eigentones in a Rectangular Chamber at Low Frequency Range," J. Acoust. Soc. Am., **10**(3), pp. 235–238.
[2] Bolt, R. H., 1939, "Frequency Distribution of Eigentones in a Three-Dimensional Continuum," J. Acoust. Soc. Am., **10**(3), pp. 228–234.
[3] Roe, G. M., 1941, "Frequency Distribution of Normal Modes," J. Acoust. Soc. Am., **13**(1), pp. 1–7.
[4] Morse, P. M., and Bolt, R. H., 1944, "Sound Waves in Rooms," Rev. Mod. Phys., **16**(2), pp. 69–150.
[5] Lord Rayleigh, 1945, *The Theory of Sound*, 2nd ed., reprinted, Dover, New York.
[6] Lyon, R. H., 1975, *Statistical Energy Analysis of Dynamical Systems*, MIT Press, Cambridge, MA.
[7] Courant, R., and Hilbert D., 1953, *Methods of Mathematical Physics*, Vol. 1, Interscience Publishers, Inc., New York.
[8] Bolotin, V. V., 1960, "The Edge Effect in the Oscillation of Shells," PMM, Moscow, **24**(5), pp. 831–843.
[9] Bolotin, V. V., 1962, "An Asymptotic Method for the Study of the Problem of Eigenvalues for Rectangular Regions," *Problems of Continuum Mechanics*, J. R. M. Radok, ed., Society for Industrial and Applied Mathematics, Philadelphia, PA, pp. 56–68.
[10] Bolotin, V. V., 1963, "On the Density of the Distribution of Natural Frequencies of Thin Elastic Shells," PMM, Moscow, **27**(2), pp. 362–364.
[11] Heckl, M., 1962, "Vibrations of Point-Driven Cylindrical Shells," J. Acoust. Soc. Am., **34**(10), pp. 1553–1557.
[12] Szechenyi, E., 1971, "Modal Densities and Radiation Efficiencies of Unstiffened Cylinders Using Statistical Methods," J. Sound Vib., **19**(1), pp. 65–81.
[13] Maymon, G., 1975, "Modal Densities of Stiffened, Axially Loaded Cylindrical Shells," J. Sound Vib., **42**(1), pp. 115–127.
[14] Ramachandran, P., and Narayanan, S., 2007, "Evaluation of Modal Density, Radiation Efficiency and Acoustic Response of Longitudinally Stiffened Cylindrical Shell," J. Sound Vib., **304**(1–2), pp. 154–174.
[15] Langley, R. S., 1992, "The Modal Density and Mode Count of Thin Cylinders and Curved Panels," J. Sound Vib., **169**(1), pp. 43–53.
[16] Manning, J. E., and Maidanik, G., 1964, "Radiation Properties of Cylindrical Shells," J. Acoust. Soc. Am., **36**(9), pp. 1691–1698.
[17] Fahy, F., 1987, *Sound and Structural Vibration: Radiation, Transmission and Response*, Academic Press, New York.
[18] Wang, C., and Lai, J. C. S., 2000, "The Sound Radiation Efficiency of Finite Length Acoustically Thick Circular Cylindrical Shells Under Mechanical Excitation I: Theoretical Analysis," J. Sound Vib., **232**(2), pp. 431–447.
[19] Wang, C., and Lai, J. C. S., 2000, "The Sound Radiation Efficiency of Finite Length Circular Cylindrical Shells Under Mechanical Excitation II: Limitations of the Infinite Length Model," J. Sound Vib., **241**(2), pp. 825–838.
[20] Xie, G., Thomson, D. J., and Jones, C. J. C., 2004, "Mode Count and Modal Density of Structural Systems: Relationships With Boundary Conditions," J. Sound Vib., **274**(3–5), pp. 621–651.
[21] Farshidianfar, A., Farshidianfar, M. H., Crocker, M. J., and Smith, W. O., 2011, "Vibration Analysis of Long Cylindrical Shells Using Acoustical Excitation," J. Sound Vib., **330**(14), pp. 3381–3399.
[22] Leissa, W., 1973, *Vibration of Shells (NASA SP-288)*, U.S. Government Printing Office, Washington, DC.
[23] Soedel, W., 1980, "A New Frequency Formula for Closed Circular Cylindrical Shells for a Large Variety of Boundary Conditions," J. Sound Vib., **70**(3), pp. 309–317.
[24] Oliazadeh, P., Farshidianfar, M. H., and Farshidianfar, A., 2013, "Exact Analysis of Resonance Frequency and Mode Shapes of Isotropic and Laminated Composite Cylindrical Shells; Part I: Analytical Studies," J. Mech. Sci. Technol., **27**(12), pp. 3635–3643.
[25] Oliazadeh, P., Farshidianfar, M. H., and Farshidianfar, A., 2013, "Exact Analysis of Resonance Frequency and Mode Shapes of Isotropic and Laminated Composite Cylindrical Shells; Part II: Parametric Studies," J. Mech. Sci. Technol., **27**(12), pp. 3645–3649.